Calculation of Invariant Manifold for Isothermal Spatially Homogeneous Reactions with Detailed Kinetics

By: Clayton R. Swope

For: Drs. Joseph M. Powers, Samuel Paolucci

AME 499: Undergraduate Research

Department of Aerospace and Mechanical Engineering

University of Notre Dame

Notre Dame, IN 46556

August 2003

Abstract

The objective of this research was to determine the concentrations of the intermediate molecular species with respect to time during the isothermal spatially homogeneous decomposition of ozone in order to identify the invariant manifold for the system. The fourteen elementary reactions of the decomposition process were identified, and the reaction rates of each constituent intermediate species were formulated from these reactions. The steady-state equilibrium conditions and an additional six non-physical critical points were determined and locally classified using eigensystem analysis. The reaction rate equations were numerically solved to produce the system response so as to predict the concentrations of the intermediate species as a function of time. The one-dimensional manifold that stretched from the stable physical steady-state equilibrium to a non-physical unstable source was identified and analyzed. The resulting analysis yielded a description of the physical reaction process for specific physical initial concentrations of the constituent elements as the elements approached the one-dimensional manifold and steady-state conditions.

1 Introduction

1.1 Combustion

The chemical processes involved in the combustion process is the focus of much study; for without a complete understanding of how the major species involved in oxidation interact over time, it is difficult to accurately model an event. The simplicity of the stoichiometric balance equations used to represent many high-temperature combustion processes, such as the decomposition of ozone, is rather deceptive in that this representation assumes the products of such a reaction are solely mixtures of ideal products. True high-temperature combustion processes usually produce numerous minor species – some in relatively large quantities – of the associated chemical components as the major chemical species tend to dissociate. An understanding of the equilibrium or steady-state of a chemical combustion process requires an understanding of how the properties of a chemical system vary with time and initial conditions.

The manner in which the amounts of the components involved in a combustion process change over time is controlled and influenced by the chemical reaction rates of the system under study. The study of these reactions and their associated chemical reaction rates is referred to as chemical kinetics. The goal of chemical kinetics is to define the specific pathways of a chemical system from initial reactants to final equilibrium products and define their reactions rates along this path. Numerical solutions that take into account the chemistry of a system are generally required to solve for these rates and generate the corresponding reaction response.

1.2 Chemical Reactions

A combustion process involving one mole of fuel *F* and *a* moles of oxidizer *O* in the formation of *b* moles of combustion product *P* is referred to as the global reaction mechanism and is represented by

$$F + aO \rightarrow bP\,. \tag{1.1}$$

The rate at which the fuel is consumed during the reaction $d[X_F]/dt$ can be modeled by the law of mass action as

$$\frac{d[X_F]}{dt} = -k_G(T)[X_F]^n[X_{Ox}]^m, \tag{1.2}$$

where $[X_i]$refers to the molar concentration of the *i*th species of the reaction, $k_G(T)$ is the global rate coefficient and is a function of temperature, and the exponents *n* and *m* are the reaction orders for a particular reaction component, [1]. The sum of the reaction orders yields the overall reaction order, and the exponents, *n* and *m*, reflect individual system components. The rate coefficient remains constant during an isothermal reaction, but varies for reactions that do not occur at a constant temperature. The negative sign preceding the rate coefficient indicates that the reaction consumes fuel and that the concentration of fuel decreases as the reaction progresses. The global reaction orders are usually integers of low order for elementary reactions.

An examination of the global reaction equation generally does not yield a substantial amount of information regarding the events that occur within a chemical reaction. Theoretically, it is possible to assume from Equation (1.1) that *a* moles of oxidizer collide with one mole of fuel to produce exactly *b* moles of product;

however, the results of experimentation indicate the presence of many intermediate species in the reaction. The elementary reactions involving these intermediate species are required to understand the dynamic behavior of a combustion process and the entire reaction mechanism.

Some chemical reactions involve dozens of elementary reactions, each with its own corresponding reaction rate and rate coefficient. Elementary reactions typically involve the collision of two molecules which result in the formation of two products. The forward bimolecular reaction can be expressed as

$$A + B \rightarrow C + D\,. \tag{1.3}$$

For example, the associated elementary reaction rate of species A or $d[A]/dt$, the rate at which the fuel is consumed during the reaction can be shown as

$$\frac{d[A]}{dt} = -k(T)[A][B]\,, \tag{1.4}$$

where $[A]$ refers to the molar concentration of species A, $[B]$ refers to the molar concentration of species B and $k(T)$ is a temperature-dependent rate coefficient. In this situation the reaction orders for each species A and B are both unity; therefore, the overall reaction order is two.

As with the global rate coefficient discussed earlier, the rate coefficient of the elementary reaction shown in Equation (1.3) is dependent on reaction temperature as represented by the Arrhenius form

$$k(T) = AT^{b}e^{-E_A/R_uT}, \tag{1.5}$$

where A is the frequency factor, b is an empirical form factor, E_a is the activation energy, T is the temperature of the reaction and R_u is the universal gas constant and equal to 8314.5 J/(kmol-K). The Arrhenius form of the rate coefficient is derived from molecular collision theory and applies as long as the temperature is not too large. Similar to bimolecular reactions, but involving only one single species undergoing an isomerization or decomposition rearrangement, unimolecular reactions can be represented by

$$\begin{matrix} A \rightarrow B \\ A \rightarrow B + C \end{matrix}. \tag{1.6}$$

For example, the associated elementary reaction rate of species A or $d[A]/dt$, the rate at which the fuel is consumed during the reaction can be represented as

$$\frac{d[A]}{dt} = -k(T)[A], \tag{1.7}$$

where $[A]$ refers to the molar concentration of species A and $k(T)$ is the rate coefficient for species A. Here the reaction order is one. The chemical kinetics of a combustion process can be ascertained by examining the global reaction mechanism and the elementary reactions involving all of the intermediate species associated with the given process. For each species involved in the reaction process, there exists a corresponding reaction rate equation that represents the rate of change of

that particular species over time based directly on the elementary reactions involved in the combustion process.

1.3 Example of the Zeldovich Mechanism

Let us examine the Zeldovich mechanism for the formations of nitric acid from atmospheric nitrogen as defined by

$$N_2 + O \xrightarrow{k_1} NO + N, \tag{1.8}$$

$$NO + N \xrightarrow{k_2} N_2 + O, \tag{1.9}$$

$$N + O_2 \xrightarrow{k_3} NO + O, \tag{1.10}$$

$$NO + O \xrightarrow{k_4} N + O_2, \tag{1.11}$$

where k_1 and k_3 are forward reaction coefficients for reaction one and three, respectively, [2]. Additionally, k_2 and k_4 are the reverse reaction coefficients for the process. The Zeldovich mechanism describes a widely studied reaction process and demonstrates the characteristics common to many reactions with multiple intermediate species present throughout the reaction. The forward global mechanism that represent the system shown in Equations (1.8 - 1.11) is

$$N_2 + O_2 \xrightarrow{k_G} 2NO. \tag{1.12}$$

An examination of the elementary reactions in Equations (1.8-1.11) indicates the presence of five intermediate species in the formation of nitric acid: NO, N, N_2, O_2 and O. Note that the global expression in Equation (1.12) that defines the initial reactions and the final products fails to account for these intermediate species and therefore is not representative of the actual chemical process.

Utilizing the four elementary reactions in Equations (1.8 - 1.11) and the law of mass action it is possible to obtain the elementary reaction rates for the process and represent them by

$$\frac{d[NO]}{dt} = k_1[N_2][O] - k_2[NO][N] + k_3[N][O_2] - k_4[NO][O], \tag{1.13}$$

$$\frac{d[N]}{dt} = k_1[N_2][O] - k_2[NO][N] - k_3[N][O_2] + k_4[NO][O], \tag{1.14}$$

$$\frac{d[N_2]}{dt} = -k_1[N_2][O] + k_2[NO][N], \tag{1.15}$$

$$\frac{d[O_2]}{dt} = -k_3[N][O_2] + k_4[NO][O], \tag{1.16}$$

$$\frac{d[O]}{dt} = -k_1[N_2][O] + k_2[NO][N] + k_3[N][O_2] - k_4[NO][O]. \tag{1.17}$$

The reaction rate for each intermediate species is itself a non-linear ordinary differential equation (ODE) whose order is equal to the largest sum of the reaction orders for each term of the rate equation. For the Zeldovich mechanism, the largest sum of the reaction orders for each of the five reaction rates is two; thus, the overall reaction order for each rate equation in this system is two.

2 Analysis Techniques

2.1 Ordinary Differential Equations

The evolution of species concentration during any reaction, like the Zeldovich mechanism, is determined by a system of ODEs. Combustion processes can be described by a system of ODEs representing the reaction rates of the intermediate species derived from the elementary reaction equations and the law of mass action. A complete solution for the ODEs will yield a description of the chemical kinetics of system evolution over time. And as with the Zeldovich mechanism, the ODEs that make up the representative system are usually stable and non-linear in nature. They also typically lack explicit, closed form, solutions. In these situations, where no closed form solution to the system is obtainable, it is necessary to compute numerical solutions to the differential equations.

Numerical solutions to systems of ODEs cannot provide an exact closed functional form to the given problem and instead produce a subset of points from the solution space. These points contain numerical errors based upon the integration routine used to perform the calculations; however, this error can be minimized by varying several computational parameters, especially the length of the time steps used in the integration and acceptable error tolerances of the routine. To obtain convergence between the theoretical closed-form solution – and mimic the real-life behavior of a chemical reaction – the distance between the individual points of the numerical solution must be small enough to reflect all variations in the system at all times scales of the reaction. Since these time-scales vary with time during any given reaction, it is important to take into account the smallest to ensure an accurate representation of the solution.

Stable systems approach a finite steady-state, while unstable systems approach infinity as time progresses. Combustion processes begin at some initial state with the initial reactants at some starting quantity and progress to steady-state over a given time. The steady-state occurs as time approaches infinity as combustion processes in closed systems can be shown to be stable. When no further changes occur in the dependent variables of the system for continued changes of the independent variables, the equilibrium state has been reached. For combustion processes, the independent variable is time and the dependent variables are the species concentrations. For example, consider the following *n*-dimensional system of *n* first-order ODEs as defined by

$$\frac{d\mathbf{x}}{dt} = \mathbf{f}(x_1, x_2, ..., x_n), \tag{2.1}$$

where the lowercase boldface letter represents a vector **f** as a function of time *t* and **x** is a vector of dependent variables composed of *n* individual variables x_i. Similarly, use of capital boldface notation denotes a matrix. The vector **f** is composed of equations that describe the rates of change of the associated dependent variables in terms of time, which varies from $0 \le t \le \infty$. If the system of equations if linear, then it may be referred to by

$$\frac{d\mathbf{x}}{dt} = \mathbf{A}\mathbf{x}, \tag{2.2}$$

where **A** is a matrix of constants. The critcal points of the system are the constant and time-independent solutions for a given set of initial conditions. The critcal points were obtained by equating $\mathbf{f}(\mathbf{x}_0) = 0$ to zero and solving for the dependent

variables at this condition. And when $\mathbf{f}(\mathbf{x}_0) = 0$, the rate of change is consequently zero at critical point $\mathbf{x}_0$. The critical points may vary with intial conditions.

2.2 Eigenvalue and Eigenvector Analysis

The Jacobian is a local linearization of the system whose components can be utilized to describe the system characteristics near a point along the solution trajectory. The local behavior of the system in Equation (2.1) can be ascertained at point $\mathbf{x}_0$ by utilizing the Jacobian **J** represented by

$$\mathbf{J} = \begin{bmatrix} \frac{\partial f_1}{\partial x_1} & \frac{\partial f_1}{\partial x_2} & \cdots & \frac{\partial f_1}{\partial x_n} \\ \frac{\partial f_2}{\partial x_1} & \frac{\partial f_2}{\partial x_2} & \cdots & \frac{\partial f_2}{\partial x_n} \\ \vdots & \vdots & \ddots & \vdots \\ \frac{\partial f_n}{\partial x_1} & \frac{\partial f_n}{\partial x_2} & \cdots & \frac{\partial f_n}{\partial x_n} \end{bmatrix}_O , \tag{2.3}$$

where the subscript *O* indicates the point $\mathbf{x}_0$ at which the Jacobian is evaluated. This point $\mathbf{x}_0$ is an arbitrary point in the phase space ***x***. Each term of the matrix represents the rates of change for each equation within the system by each dependent variable $\mathbf{x}_i$ in terms of the independent variable and the remaining dependent variables. If $\mathbf{x}_0$ is chosen to be a critical point which is defined as $\mathbf{f}(\mathbf{x}_0) = 0$, then the real positive eigenvalues resulting from the Jacobian matrix in Equation (2.3) indicate that the given critical point of the system is unstable. Note, this analysis applies strictly to two-dimensional systems; however, similar extensions can be made for systems of higher dimensions. Real eigenvalues of opposite signs indicate that the given critical point of the system is an unstable saddle point. Imaginary components to these critical points indicate that the

solution possesses an oscillatory component near the critical point with either a stable or unstable spiral depending on the sign of the real part of the eigenvalues. Real negative or positive eigenvalues indicate that the given point of the system is a sink or source, respectively.

As mentioned before, the physical combustion processes modeled by a system of ODEs are stable and thus approach some final equilibrium condition; however, the differential equations used to model these physical processes may in fact possess additional critical points that may lie in the non-physical region of the phase space. For example, a system of ODEs that models a given combustion process may contain a stable equilibrium with one or more negative coordinates in the phase plane. Even though laboratory experiments could never produce negative species concentrations, understanding these non-physical critical points can yield important insights that relate to the physical behavior of the combustion process represented within the physical region of the space.

The amount of computational time and effort required to execute a numerical solution depends directly on the exact nature of the ODE system, especially its stiffness. I am restricting my discussion to systems with strictly real eigenvalues and that suitable extensions exist for systems with complex eigenvalues; therefore, $\lambda_1, \lambda_2, ..., \lambda_n$ are the eigenvalues of a system of ODEs, the stiffness S is

$$S = \frac{\max|\lambda|}{\min|\lambda|}. \tag{2.4}$$

2.3 System Time-Scale and Manifold Identification

The local set of time-scales that describe the reaction rates of the elementary reactions that occur within a combustion process are represented by the eigenvalues

of the Jacobian of the ODE system. For systems with real eigenvalues the reaction time scales are equal to the reciprocals of the eigenvalues of the Jacobian matrix. The solution *x(t)* with respect of time *t* resulting from a system of two ODEs with two non-equal eigenvalues is

$$x(t) = Ae^{\lambda_1 t} + Be^{\lambda_2 t}, \tag{2.5}$$

where *A* and *B* are constants. Negative eigenvalues indicates that the system exponentially approaches a steady-state value. Positive eigenvalues indicates that the system exponentially grows towards some an infinite unstable value. The non-zero imaginary components of the eigenvalues, if they exist, define the frequency and the time-scale of the oscillatory component of the system near that point. The eigenvectors of the Jacobian indicates the instantaneous direction of the solution trajectory at a certain point in the phase space.

In instances where the difference between the smallest and longest time-scale is on the order of several magnitudes, the information contained in the solution for the reaction rate equation relating to the smallest time-scale is the most important and can be used to classify the behavior of the entire system. The behavior of the system characterized by the slowest time-scale is often the most important of the system because it is that behavior that is most easily observed in the physical results and represented in laboratory data for a given combustion process. The fastest time-scale components of the system equilibrate onto what is termed a low-dimensional manifold; therefore, since it is the slow time-scale components that determine the nature of this low-dimensional manifold, the slow time-scale components uniquely define the long term system response.

Consider that an *n*-dimensional manifold is a space in *n* dimensions. A point is a zero-dimensional manifold, while a line is a one-dimensional manifold. For

example, the solution trajectories that describe the species concentration for a combustion reaction throughout time begin at time zero at a set of given initial concentrations. Those initial concentrations determine the unique behavior and characteristics of the solution trajectories in the phase space of the system as the concentrations approach a steady-state for those specific initial conditions. For any initial conditions within a certain region of the phase space, all the solution trajectories approach the steady-state equilibrium point. This equilibrium condition, a point in the phase space, is the zero-dimensional manifold for the system and achieved as time approaches infinity.

The solution trajectories approach a one-dimensional manifold, or the one-dimensional path, at times when the slowest of the system time-scales dominates the response. The one dimensional path is common to all solutions, for a given set of initial conditions, in a certain region of the phase space. The two-dimensional manifold is the two-dimensional surface that the trajectories approach from the same initial conditions when the two longest time-scale dominate the responses. The three-dimensional manifold and other higher order manifolds are defined similarly and depend on the relative magnitude of the time-scales that currently dominate the system response at each point.

As time approaches infinity, the location of the solution trajectories become confined to smaller dimensions – as long as all initial conditions reside in a similar region of the phase space – until all trajectories end at one point, the equilibrium condition. The ability of a manifold to accurately describe a particular solution is determined by the dimension of the manifold and related directly to the time that has passed in the reaction. The system response of a stable system initially dominated by a fast time-scale will approach a low-dimensional manifold as time progresses and finally reach the steady-state, the zero-dimensional manifold.

In general, as time progresses, the solution trajectories approach the manifolds more closely, but never actually lie on the manifold itself. This observation holds true for all initial conditions that fall within the region of the phase space where trajectories approach the same equilibrium condition as time approaches infinity. Initial conditions in different regions of the phase space may approach different equilibrium conditions with different solution trajectories and associated manifolds. The only instance when a solution trajectory falls on the manifold itself occurs when the initial conditions lie on the manifold. The solution trajectory for a set of initial conditions on the manifold never leaves the manifold as the system approaches the equilibrium state.

For a given set of initial conditions, all trajectories eventually approach a zero-dimensional manifold, or equilibrium condition, as time approaches infinity and if a set of initial conditions happens to reside on a manifold, the resulting solution trajectory will never leave that manifold. Thus if a set of initial conditions happens to correspond to an equilibrium point of a system, the solution trajectory will simply remain at that point. The equilibrium condition is the initial condition. For a combustion process, the initial species concentration will not change, regardless of how much time elapses for the reaction process. Accordingly, if a set of initial conditions lies on the one-dimensional manifold, it will follow the one-dimensional path of that manifold to the equilibrium point assuming a stable equilibrium.

3 Analysis of Ozone Decomposition

3.1 Reaction Characteristics

The three species, fourteen step reaction mechanism for the decomposition of ozone was studied, [4]. The fourteen steps, or intermediate reactions, consisted of the following, listed respectively

$$O_3 + O \xrightarrow{k_1} O_2 + 2O, \tag{3.1}$$

$$O_2 + 2O \xrightarrow{k_2} O_3 + O, \tag{3.2}$$

$$O_3 + O_2 \xrightarrow{k_3} 2O_2 + O, \tag{3.3}$$

$$2O_2 + O \xrightarrow{k_4} O_3 + O_2, \tag{3.4}$$

$$2O_3 \xrightarrow{k_5} O_2 + O + O_3, \tag{3.5}$$

$$O_2 + O + O_3 \xrightarrow{k_6} 2O_3, \tag{3.6}$$

$$O + O_3 \xrightarrow{k_7} 2O_2, \tag{3.7}$$

$$2O_2 \xrightarrow{k_8} O + O_3, \tag{3.8}$$

$$O_2 + O \xrightarrow{k_9} 3O, \tag{3.9}$$

$$3O \xrightarrow{k_{10}} O_2 + O, \tag{3.10}$$

$$2O_2 \xrightarrow{k_{11}} 2O + O_2, \tag{3.11}$$

$$2O + O_2 \xrightarrow{k_{12}} 2O_2, \tag{3.12}$$

$$O_2 + O_3 \xrightarrow{k_{13}} 2O + O_3, \tag{3.13}$$

$$2O + O_3 \xrightarrow{k_{14}} O_2 + O_3, \tag{3.14}$$

where k_i indicates the reaction coefficient for each reaction. The three intermediate components in this combustion process are O, O_2 and O_3. The system was assumed

to be a well-stirred, isothermal reaction; thus, the three elementary reaction rates for each of these intermediate species were obtained from the law of mass action. The reaction rates for the Zeldovich mechanism were obtained earlier by utilizing the same assumptions. The reaction rate, or kinematic, equations are

$$\begin{aligned}\frac{d[O]}{dt} &= k_1[O][O_3] - k_2[O]^2[O_2] + k_3[O_2][O_3] - k_4[O][O_2]^2 + k_5[O_3]^2 \\ &- k_6[O][O_2][O_3] - k_7[O][O_3] + k_8[O_2]^2 + 2k_9[O][O_2] - 2k_{10}[O]^3 + 2k_{11}[O_2]^2 , \\ &- 2k_{12}[O]^2[O_2] + 2k_{13}[O_2][O_3] - 2k_{14}[O]^2[O_3]\end{aligned} \tag{3.15}$$

$$\begin{aligned}\frac{d[O_2]}{dt} &= k_1[O][O_3] - k_2[O]^2[O_2] + k_3[O_2][O_3] - k_4[O][O_2]^2 + k_5[O_3]^2 \\ &- k_6[O][O_2][O_3] + 2k_7[O][O_3] - 2k_8[O_2]^2 - k_9[O][O_2] + k_{10}[O]^3 - k_{11}[O_2]^2 , \\ &+ k_{12}[O]^2[O_2] - k_{13}[O_2][O_3] + k_{14}[O]^2[O_3]\end{aligned} \tag{3.16}$$

$$\begin{aligned}\frac{d[O_3]}{dt} &= -k_1[O][O_3] + k_2[O]^2[O_2] - k_3[O_2][O_3] + k_4[O][O_2]^2 - k_5[O_3]^2 \\ &+ k_6[O][O_2][O_3] - k_7[O][O_3] + k_8[O_2]^2\end{aligned} . \tag{3.17}$$

The reaction rate coefficients were determined by utilizing the Arrhenius form of Equation (1.5). The reaction temperature was assumed to be 3000 K.

The constants A and b along with the activation energies E_A for each reaction are shown in Table 1. These constants were used in conjunction with Equation (1.5) to obtain the reaction coefficients for the decomposition. The units of A were chosen such that the reaction rates achieve the units of mole/cm^3/s.

Reaction	***A***	***b***	***E_A [kJ/mol]***
1	6.76×10^6	2.50	1.01×10^{12}
2	1.18×10^2	3.50	0.00
3	6.76×10^6	2.50	1.01×10^{12}
4	1.18×10^2	3.50	0.00
5	6.76×10^6	2.50	1.01×10^{12}
6	1.18×10^2	3.50	0.00
7	4.58×10^6	2.50	2.51×10^{11}
8	1.88×10^6	2.50	4.15×10^{12}
9	5.71×10^6	2.50	4.91×10^{12}
10	2.47×10^2	3.50	0.00
11	5.71×10^6	2.50	4.91×10^{12}
12	2.47×10^2	3.50	0.00
13	5.71×10^6	2.50	4.91×10^{12}
14	2.47×10^2	3.50	0.00

Table 1: Values of A, b and E_A for each intermediate reaction, [3].

The reaction system shown in Equations (3.15-3.17) can be written in the matrix form

$$\begin{Bmatrix} \frac{d[O]}{dt} \\ \frac{d[O_2]}{dt} \\ \frac{d[O_3]}{dt} \end{Bmatrix} = \mathbf{C} \cdot \mathbf{D} . \tag{3.18}$$

The matrix **C** is defined as

$$\mathbf{C} = \begin{bmatrix} 1 & -1 & 1 & -1 & 1 & -1 & -1 & 1 & 2 & -2 & 2 & -2 & 2 & -2 \\ 1 & -1 & 1 & -1 & 1 & -1 & 2 & -2 & -1 & 1 & -1 & 1 & -1 & 1 \\ -1 & 1 & -1 & 1 & -1 & 1 & -1 & 1 & 0 & 0 & 0 & 0 & 0 & 0 \end{bmatrix}, \qquad (3.19)$$

and the matrix **D** composed of the rate coefficients and intermediate reaction species components is defined as

$$\mathbf{D} = \begin{Bmatrix} k_1[O][O_3] \\ k_2[O]^2[O_2] \\ k_3[O_2][O_3] \\ k_4[O][O_2]^2 \\ k_5[O_3]^2 \\ k_6[O][O_2][O_3] \\ k_7[O][O_3] \\ k_8[O_2]^2 \\ k_9[O][O_2] \\ k_{10}[O]^3 \\ k_{11}[O_2]^2 \\ k_{12}[O]^2[O_2] \\ k_{13}[O_2][O_3] \\ k_{14}[O]^2[O_3] \end{Bmatrix}. \qquad (3.20)$$

The three differential equations are autonomous functions. The system is non-linear with a reaction order of three.

3.2 Simplifications and Constraints

The form of the matrix resulting from **C**·**D** represented in Equation (3.18) can be simplified by performing row operations on the matrix to reduce matrix **C** to row-echelon form according to

$$\begin{Bmatrix} \frac{dx_1}{dt} \\ \frac{dx_2}{dt} \\ \frac{dx_3}{dt} \end{Bmatrix} = \begin{Bmatrix} \frac{d[O]}{dt} + \frac{d[O_2]}{dt} + \frac{d[O_3]}{dt} \\ \frac{d[O_2]}{dt} + \frac{d[O_3]}{dt} \\ \frac{d[O]}{dt} + 2\frac{d[O_2]}{dt} + 3\frac{d[O_3]}{dt} \end{Bmatrix} = C_{new} \cdot D . \tag{3.21}$$

The resulting matrix $\mathbf{C}_{\text{new}}$ in row-echelon form is

$$\mathbf{C}_{new} = \begin{bmatrix} 1 & -1 & 1 & -1 & 1 & -1 & 0 & 0 & 1 & -1 & 1 & -1 & 1 & -1 \\ 0 & 0 & 0 & 0 & 0 & 0 & 1 & -1 & -1 & 1 & -1 & 1 & -1 & 1 \\ 0 & 0 & 0 & 0 & 0 & 0 & 0 & 0 & 0 & 0 & 0 & 0 & 0 & 0 \end{bmatrix}. \tag{3.22}$$

These resulting three differential equations, now in a new x_1-x_2-x_3 phase space, indicate that

$$\frac{dx_3}{dt} = \frac{d[O]}{dt} + 2\frac{d[O_2]}{dt} + 3\frac{d[O_3]}{dt} = 0 . \tag{3.23}$$

Integrating the expression in Equation (3.23) yields

$$x_3 = [O]_i + 2[O_2]_i + 3[O_3]_i , \tag{3.24}$$

where the term x_3 is constant throughout the process. Given a specific set of initial concentrations, the algebraic constraint of Equation (3.24) can be used to express x_3 and thus the concentration of [O_3] in terms of the concentrations of [O] and [O_2] at

any time during the combustion process. The value of x_3 at the initial conditions can be obtained by utilizing Equation (3.24) for a given set of initial concentration and according to Equation (3.23) and Equation (3.24), that value remains constant throughout the combustion process. The resulting expression for the concentration of $[O_3]$ in terms of the concentrations of $[O]$ and $[O_2]$ is

$$[O_3] = \frac{[O]_i + 2[O_2]_i + 3[O_3]_i - [O] - 2[O_2]}{3}, \tag{3.25}$$

where $[O]_i$, $[O_2]_i$ and $[O_3]_i$ are the initial concentrations of $[O]$, $[O_2]$ and $[O_3]$, respectively. The expression for the concentration of $[O_3]$ in Equation (3.25) becomes

$$[O_3] = \frac{2.7419682 \times 10^{-5} - [O] - 2[O_2]}{3}, \tag{3.26}$$

when the concentrations listed in Table 2 are utilized.

$[O]_i$ [mol/cm³]	$[O_2]_i$ [mol/cm³]	$[O_3]_i$ [mol/cm³]
0.00	0.00	$(2.741982 / 3) \times 10^{-5}$

Table 2: Initial vales for the concentrations [O], [O_2] and [O_3].

By utilizing Equation (3.26), the three differential equations listed in Equations (3.15-3.17) in terms of $[O]$, $[O_2]$ and $[O_3]$ can be reduced to two differential equations in terms of variable x_1 and x_2. In the new x_1-x_2-x_3

$$x_3 = \frac{2.7419682 \times 10^{-5} - x_1 - 2x_2}{3}. \tag{3.27}$$

The two reduced and simplified differential equations become

$$\frac{dx_1}{dt} = \left(\frac{2.7419682\times10^{-5} - x_1 - 2x_2}{3} \right)\left(k_1 x_1 + k_3 x_2 - k_6 x_1 x_2 + k_{13} x_2 - k_{14} x_1^{\,2}\right)$$
$$- k_5\left(\frac{2.7419682\times10^{-5} - x_1 - 2x_2}{3} \right)^2 - k_2 x_1^{\,2} x_2 - k_4 x_1 x_2^{\,2} + k_9 x_1 x_2 \quad , \qquad (3.28)$$
$$- k_{10} x_1^{\,3} + k_{11} x_2^{\,2} - k_{12} x_1^{\,2} x_2$$

$$\frac{dx_2}{dt} = \left(\frac{2.7419682\times10^{-5} - x_1 - 2x_2}{3} \right)\left(k_7 x_1 - k_{13} x_2 + k_{14} x_1^{\,2}\right) - k_8 x_2^{\,2} - k_9 x_1 x_2 + k_{10} x_1^{\,3} \quad . \qquad (3.29)$$
$$- k_{11} x_2^{\,2} + k_{12} x_1^{\,2} x_2$$

Both Equation (3.28) and Equation (3.29) were derived using the initial conditions in Table 2; therefore, resulting solutions of x_1 and x_2 only correspond to physical concentrations of *[O]* and $[O_2]$ for those initial values. The resulting trajectories and low-dimensional manifolds for other initial conditions do not correspond to physical responses of the system. The low-dimensional manifold found and discussed in later sections applies only to this set of initial conditions in Table 2.

3.3 Critical Points

The critical points, or roots, of the two differential equations for dx_1/dt and dx_2/dt in Equations (3.28 - 3.29), respectively, were obtained by setting each expression to zero and solving for the corresponding values of x_1 and x_2 simultaneously at that condition.

The seven roots to the two equations are listed in Table 2.

point	x_1 ***[mol/cm³]***	x_2 ***[mol/cm³]***
1	$1.82956413375383 \times 10^{-12}$	$-2.74196858174691 \times 10^{-5}$
2	$-2.74196839879049 \times 10^{-5}$	$2.74196858174691 \times 10^{-5}$
3	-0.221933277630227	2219578.43997629
4	$-9.43552870455286 \times 10^{-6}$	$1.8427552960238 \times 10^{-5}$
5	$-5.57102200570931 \times 10^{-7}$	$1.39884272357373 \times 10^{-5}$
6 *(physical)*	$5.4523034383475 \times 10^{-7}$	$1.34371928482426 \times 10^{-5}$
7	80.8033083728895	-168.786508474242

Table 3: Critical points of Equations (3.28 - 3.29).

The eigenvalues of the Jacobian matrix obtained from Equations (3.28 - 3.29) and calculated at the critical points listed in Table 3 can be utilized to classify the critical points according to their local behavior. All of the eigenvalues are real. These classifications can be used to determine the stability of each critical point. The classification of each critical point according to the eigenvalue analysis is listed in Table 4.

point	***type***	***stability***
1	saddle	unstable
2	saddle	unstable
3	sink	stable
4	source	unstable
5	saddle	unstable
6 *(physical)*	sink	stable
7	source	unstable

Table 4: Critical point classifications.

These seven roots of Equations (3.28 - 3.29) define the equilibrium points of the decomposition process of ozone. All seven points are real and contain no imaginary components. Two points are stable equilibrium points, while the other five are all

unstable; however, of the seven points, only one represents the physical decomposition process. Only the sixth equilibrium point contains positive values and thus represents the physical process. The other six contain at least one negative component. Negative components indicate negative concentrations. There can be no negative concentrations in the physical system at any time throughout the decomposition process. Only the sixth critical point with two positive components indicates the concentrations that the system will equilibrate to steady-state as time approaches infinity.

3.4 Space Transformations

The critical points vary in several orders of magnitude and contain both negative and positive values; therefore, in order to obtain a simple plot of the solution trajectories near each critical point on a global scale, it is necessary to transform the results into a different space.

A convenient transformation from the x_1-x_2 phase space to the $\rho - \theta$ space was achieved by the following

$$\rho = \frac{1}{2}\ln\left(x_1^{\,2} + x_2^{\,2}\right), \quad -\infty < \rho < \infty \tag{3.31}$$

$$\theta = \arctan\left(\frac{x_2}{x_1}\right), \qquad -\pi/2 < \theta < \pi/2 \tag{3.32}$$

The reaction rates in Equations (3.28 - 3.29) were then solved for the new rates $d\rho/dt$ and $d\theta/dt$. The local linearized behavior and stability characteristics are the same for each respective critical point in the new space as they were in the original space; therefore, the conditions in Table 4 still hold for each point.

The critical points in the $\rho - \theta$ phase space are listed in Table 5.

point	ρ	θ
1	-10.5042493420479	-1.57079626007042
2	-10.1576757851301	-0.785398196759688
3	14.6128278439141	-1.57079622680596
4	-10.7852439550598	-1.09756814317026
5	-11.1764877719111	-1.53099142733861
6 *(physical)*	-11.2166615727181	1.53024236454978
7	5.23180960493588	-1.12430835749168

Table 5: Critical points of Equations (3.28 - 3.29) in the $\rho - \theta$ space.

The critical points, represented by square markers, are shown superimposed on the new phase space in Figure 3.

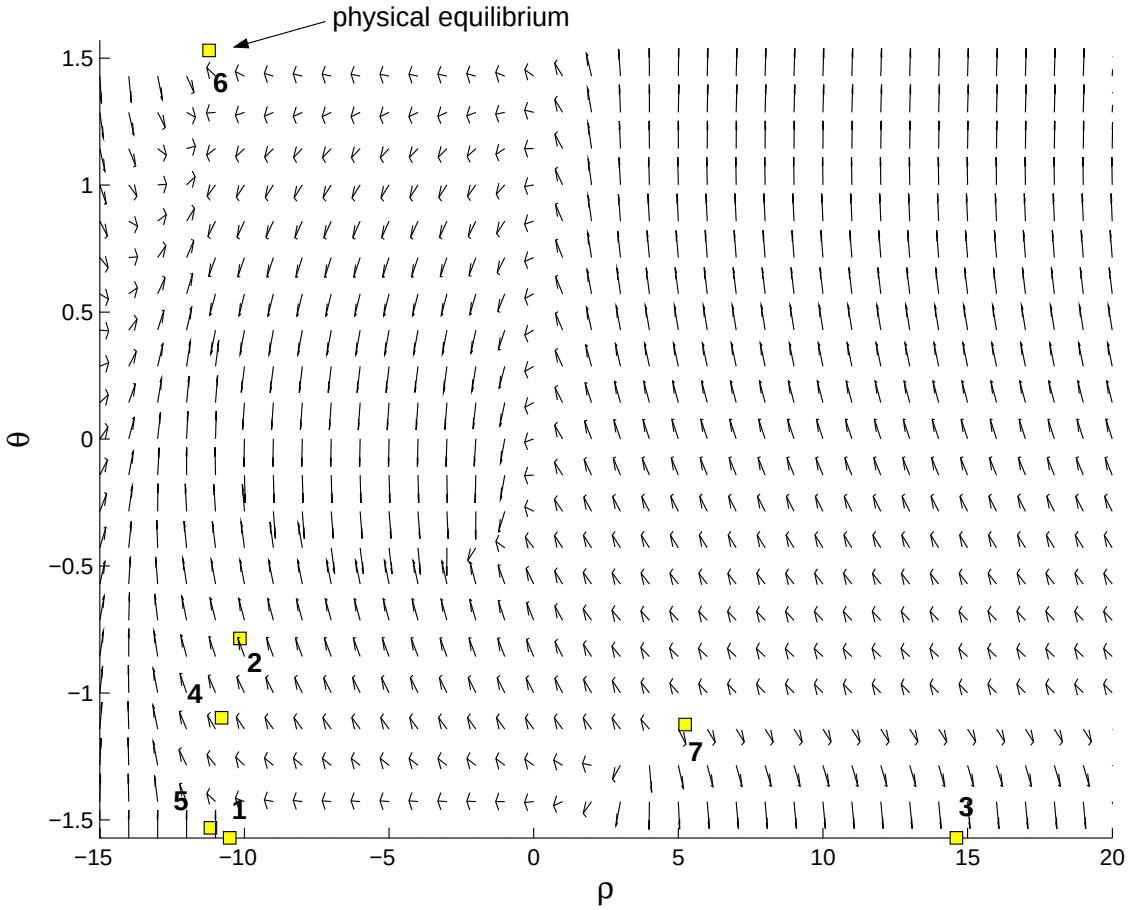

Figure 1: System phase plot in the $\rho - \theta$ *space.*

The trajectories of produced by several initial values of x_1 and x_2 are shown in Figure 2. The square markers denote the equilibrium points located in this region of the space with the position of the physical equilibrium denoted individually.

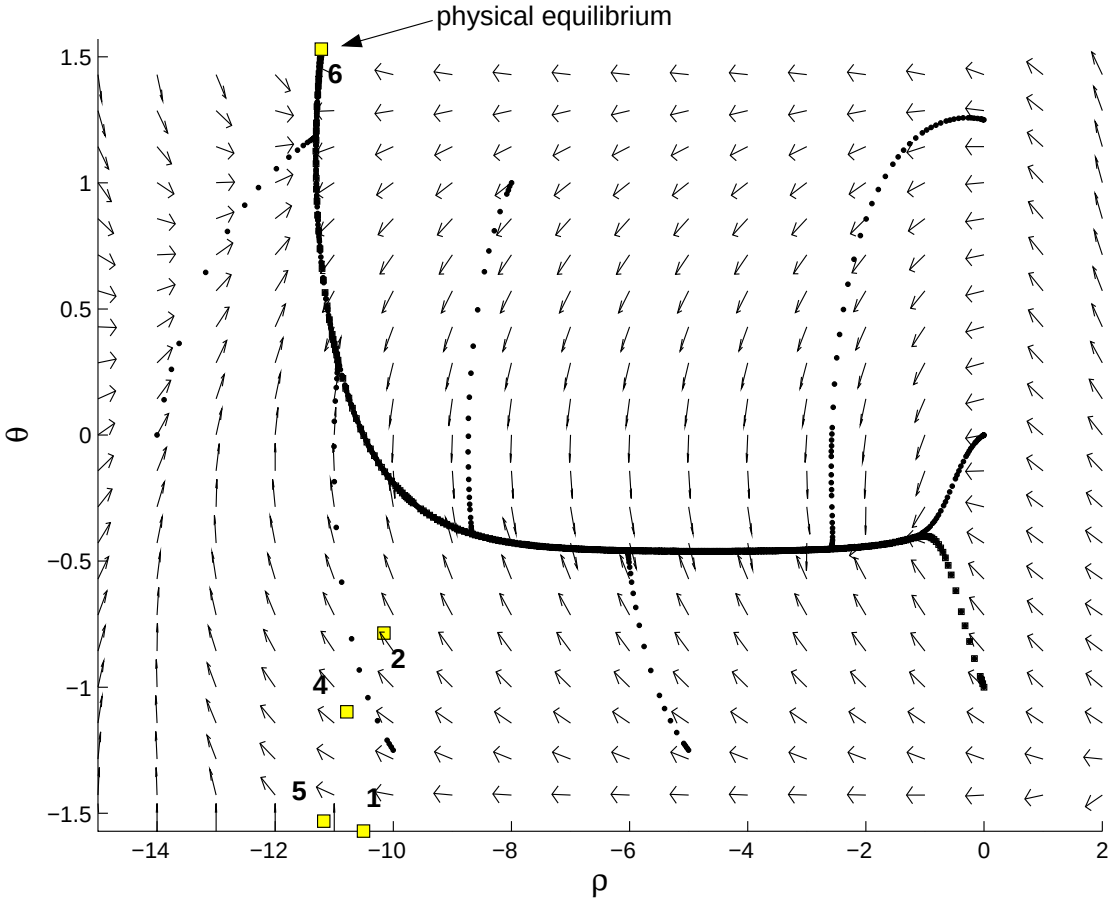

Figure 2: System response in the $\rho - \theta$ space near the physical critical point.

Again, Equations (3.28 - 3.29) were derived using the initial conditions in Table 2; therefore, the resulting system response for x_1 and x_2 correspond to physical concentrations of $[O]$ and $[O_2]$ for those initial values. Utilizing the initial concentrations in Table 2 for the initial values of x_1 and x_2 produced the system response of the concentrations of $[O]$, $[O_2]$ and $[O_3]$ versus time.

The concentration of $[O_3]$ was derived from the algebraic constraint in Equation (3.25). The system evolution is plotted in Figure 3.

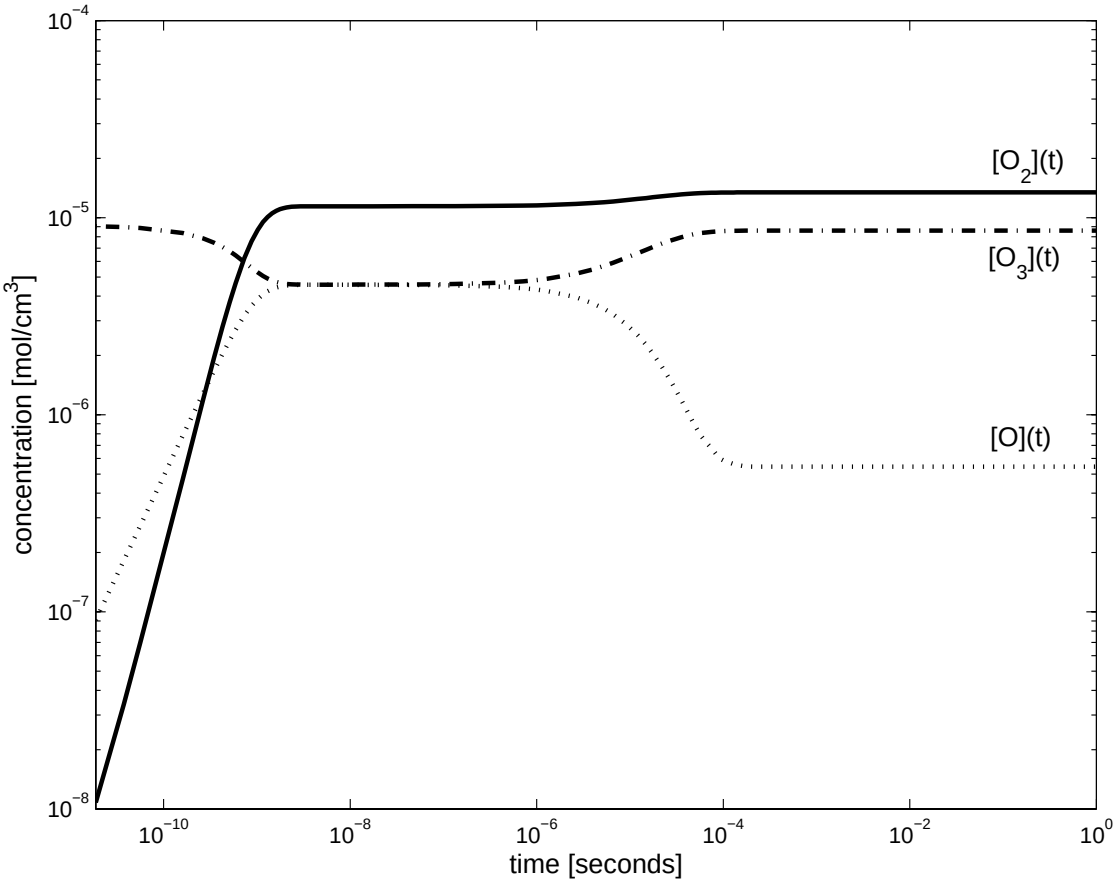

Figure 3: Concentrations of [O], $[O_2]$ and $[O_3]$ versus time for initial conditions in Table 2.

The final steady-state equilibrium values achieved for the initial conditions in Table 2 are listed in Table 6.

[O] [mol/cm³]	***$[O_2]$ [mol/cm³]***	***$[O_3]$ [mol/cm³]***
5.4523034×10^{-7}	1.3437193×10^{-5}	8.5947097×10^{-6}

Table 6: Steady-state equilibrium vales for the concentrations [O], $[O_2]$ and $[O_3]$.

3.5 System Response

The trajectories all approach the same steady-state equilibrium point as time increases. This point is the one physical equilibrium point. This point is a stable sink, meaning that for any set of physical initial values of x_1 and x_2, the values of x_1 and x_2 will approach the physical equilibrium values as time approaches infinity since the system models the real combustion process of ozone. Physical initial concentrations will not lead to negative non-physical results in the laboratory. The eigenvalues and associated eigenvectors evaluated at the physical equilibrium point indicate the time-scale and approach direction of the trajectories near the equilibrium point. This same analysis technique applied at each time increment along the solution trajectory will yield the time-scale at each point on the trajectory.

As time approaches infinity, the corresponding time-scale increases towards a finite value as the corresponding eigenvalue approaches a finite negative value. The solution approaches the zero-dimension manifold, one point, in the phase space. Before the trajectories in Figure 2 reach the zero-dimensional manifold, the equilibrium point, they approach the one-dimensional manifold. This manifold is a line in the phase space and observable in Figure 2. The trajectories approach this line when slow time-scales dominate the system. As the dominat time-scale length decreases, the resulting manifolds increase in dimension and become impossible to represent via the phase plot; therefore, the most important manifold and most easily understood is a low-dimensional manifold.

None of the initial conditions used to generate the trajectories displayed in Figure 2 lie on the low-dimensional manifold. If an initial value lies on a manifold, the resulting solution response will not deviate from that manifold. For example, if a set of initial conditions corresponded precisely with the physical equilibrium point, the resulting solution trajectory would never deviate from that point at any time. The

solution trajectory would be simply a point. Similarly, if a set of initial conditions corresponded to a point on the manifold, the resulting solution trajectory would mimic the space, a curve in this case, that defines that particular manifold.

The unstable source must terminate at another critical point, since all trajectories must end at a critical point; therefore, the length of the manifold is finite, for it must stretch between a source and a sink unless one of those critical points is infinity. In the case of the manifold in Figure 2, the starting point of the manifold lies at the unstable source, or seventh critical point listed in Table 3, and terminates at the stable physical equilibrium point. This manifold is pictured in Figure 4.

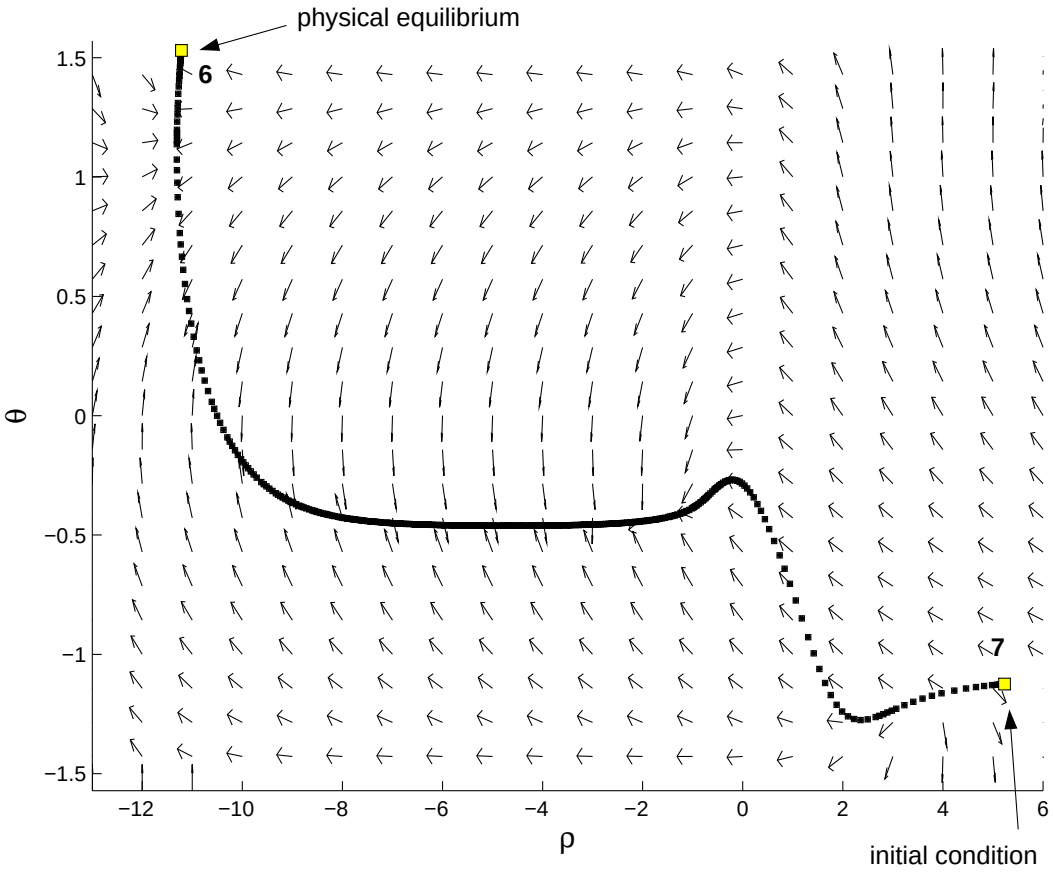

Figure 4: Manifold between the physical sink and unstable source.

As discussed earlier, trajectories approach this manifold when the response is dominated by slowest time-scales. The solution components with faster time-scales are thus dominated by the slowest time-scale component and quickly approach the low-dimensional manifold. The eigenvectors at each point in the space indicate the local system response direction. Given that the magnitude of the time-scale corresponds to the inverse of each component of the associated eigenvalues, the largest eigenvalue corresponding to the slowest time-scale of the system would indicate the local behavior – notably the direction of the trajectory – for the response.

3.6 Manifold Description

To determine the nature of the manifold between the stable physical equilibrium and the unstable source, the initial concentrations must be such that they nearly, but not precisely, equal to the coordinates of the source in the space. Since the source is a critical point of the system, it is also a zero-dimensional manifold; yet, unlike the physical sink, this manifold is in fact repelling and can be demonstrated so by calculating the eigenvectors at that point. The initial conditions must thus fall slightly away from this critical point.

A local linearized perturbation was used to obtain a new set of initial conditions. If the initial x_1 is selected arbitrarily by utilizing a small change between this condition and the x_1 condition at the source, the corresponding x_2 can be determined by setting the slope for a line. For this point to reside on the one-dimensional manifold as desired, the slope must be equal to that of the eigenvector which has the least negative eigenvalue indicative of the slowest time-scale. Since the eigenvalues are inversely proportional to the time-scales, the smallest of the eigenvalues would correspond to the slowest time-scale. And since the sink is repelling, the eigenvector is negative and the slope of the line is indeed negative as well. The sink location and initial conditions located on the one-dimensional manifold are listed in Table 7.

point	ρ	θ
7 (sink)	5.23180960493587	-1.12430835749168
initial conditions	5.23167169426310	-1.12424400000000

Table 7: Sink location and initial conditions located on the one-dimensional manifold.

The manifold extending from the unstable source to the stable sink is shown in Figure 4. The evolution of the ρ and θ concentrations in $\rho - \theta$ space versus time for initial conditions in Table 7 is shown in Figure 5.

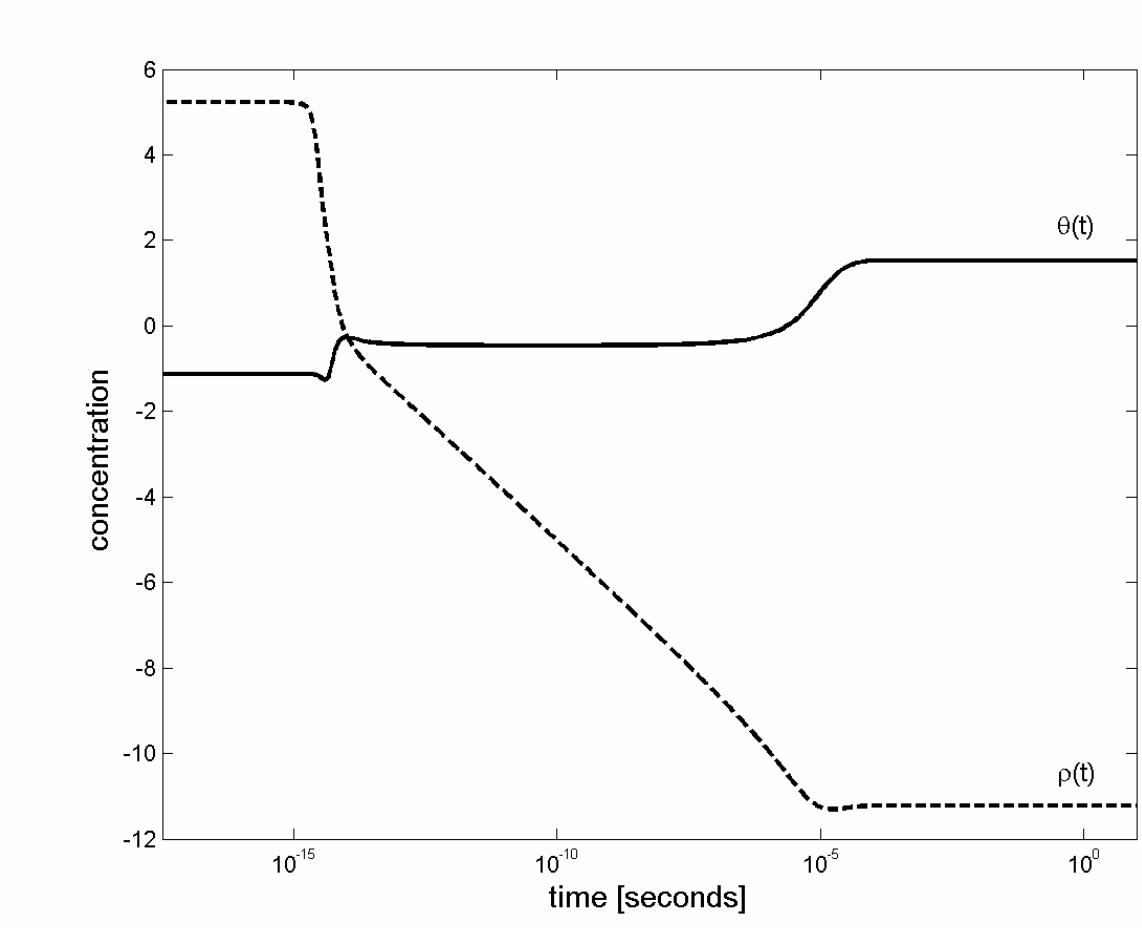

Figure 5: The concentrations in $\rho - \theta$ space versus time for initial conditions in Table 7.

Regions of the manifold can be classified according to their relative attractiveness. The attractiveness of the manifold is reflected in the size of the time-scales for the

trajectories as they approach the one-dimensional manifold from a given set of initial conditions. The smaller the reaction time from initial conditions to individual solution convergence to the manifold, the more attractive the manifold is for that particular region. Regions of the manifold can also repel solution trajectories away from convergence with the manifold for that region; therefore, the only trajectories that would follow this type of manifold originated on with initial conditions on the actual manifold.

The eigenvalues evaluated at every point along the manifold were used to determine the attractiveness of the manifold at each particular point. The norm, taken with respect to the largest eigenvalue, of the difference between the two eigenvalues determined the magnitude of the attractiveness and the sign of the difference determined the direction of its effects – positive indicates a repulsive tendency and negative indicates an attractive nature. Consider an example involving two eigenvalues, λ_1 and λ_2, of different values. Assume that the largest of the pair is always denoted as λ_1 and the smallest is always referred to as λ_2. Then the magnitude and direction of the indicator of attractiveness at the particular point with eigenvalues of λ_1 and λ_2 is *H*. For example, in the case where λ_1 and λ_2 are both real and negative, *H* is defined as

$$H = \frac{\lambda_1 - \lambda_2}{\lambda_1}. \tag{3.33}$$

In the case where λ_1 and λ_2 are both real and positive, *H* is defined as

$$H = \frac{\lambda_1 - \lambda_2}{\lambda_2}. \tag{3.34}$$

Figure 6 shows how the attractiveness of the manifold varies along the manifold length. The relative magnitude of the attractiveness or repulsiveness along the

manifold is presented as a log-magnitude. The positive region to the right of the origin denotes repulsion. The magnitude zero constant region near the origin represents a neutral attractiveness. The negative region to the left of the origin denotes attraction.

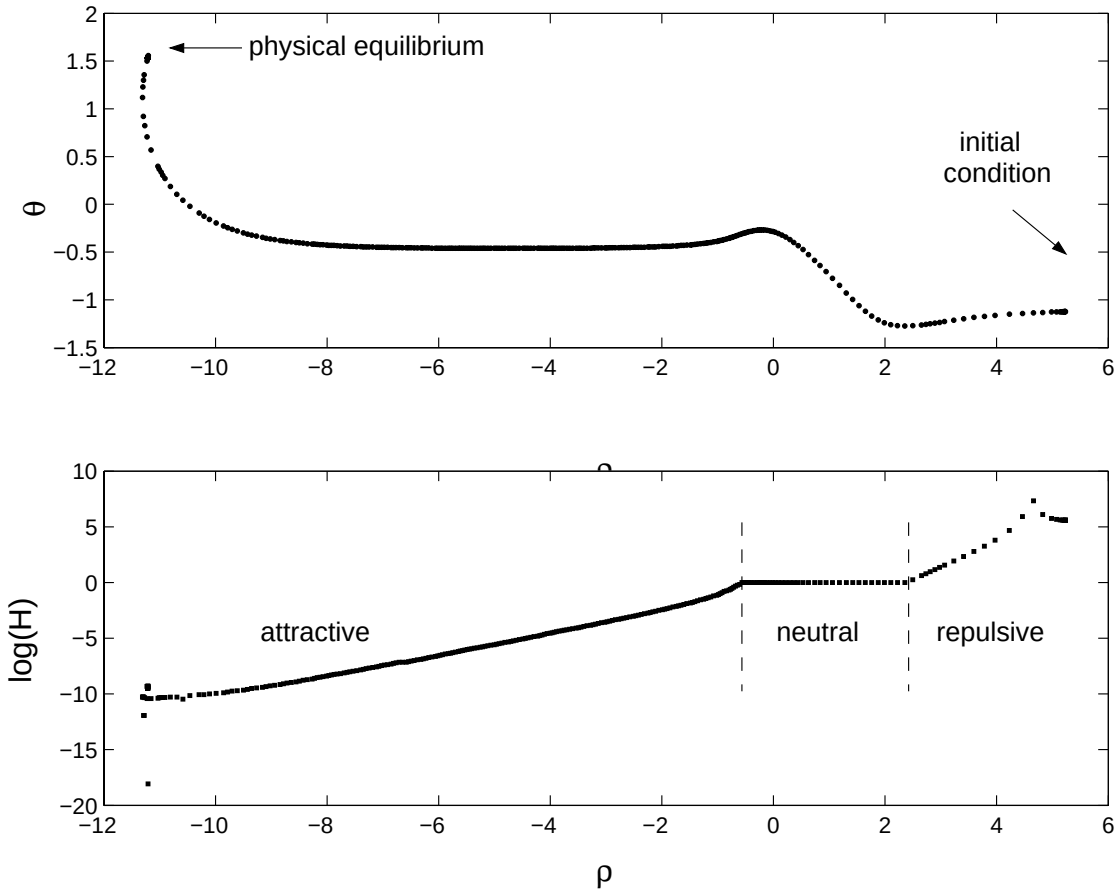

Figure 6: Manifold between the physical sink and unstable source and log-magnitude attractiveness.

3 Conclusions

The concentrations of the intermediate molecular species with respect to time during the isothermal spatially homogeneous decomposition of ozone were utilized to identify and determine the behavior of the invariant manifold for the system located between the unstable source and stable physical equilibrium conditions. The eigensystem analysis used to ascertain the attractiveness of the manifold at every point along this manifold indicates that the manifold contains a repulsive tendency near the source and gradually increases in attractiveness as the system response approaches the physical equilibrium, or steady-state condition.

The reduction of the three elementary reaction rate equations for the three intermediate elements of the reaction into two equations and the utilization of the algebraic constraint obtained from linear operations on the elementary reaction rate equations greatly simplified the integration routine. The algebraic constraint reduced the number of dependent variables from three representing the concentrations of O, O_2 and O_3 to two representing the concentrations of O and O_2 for the prescribed initial conditions used in the algebraic constraint to simplify the equations. This simplification also reduced the size of the phase space and confined the system trajectories to a two-dimensional plane whereas before the system response existed in three-dimensional space. Since numerical integration techniques were used to obtain the system response, the approach discussed and outlined herein provides a representation of the chemical kinetics of a combustion process of the system represented by two non-linear ODEs.

Analysis indicated the existence of seven critical points of the elementary reaction rate equations. All were wholly real without any imaginary components and two points were stable sinks. Only one point represented an actual physical state that

the reaction may achieve. This equilibrium point represented the steady-state condition for the reaction. The system response and critical points were transformed from the x_1-x_2 phase space into the new $\rho - \theta$ space to facilitate the analysis on a global level. System response trajectories were generated in the phase space and utilized to determine the location and appearance the one-dimensional manifold between the physical stable sink and unstable source. The computational time required to perform the numerical integrations was minimal due to the simplified nature of the rate equations through the imposition of the algebraic constraint and reduction in dependent variables. This technique provided an accurate picture of the system response and invariant manifold characteristics for the decomposition of ozone, as the only error introduced into the system response arose from the precision limitations of the computational routine.

References

1. Turns, S. R., *An Introduction to Combustion: Concepts and Applications*, pp. 111-143, McGraw-Hill, (2000).
2. Glassmaker, N. J., "ILDM Method for Rational Simplification of Chemical Kinetics," AME 499 Fluids Report, University of Notre Dame, (1999).
3. Singh, S., Powers, J. M., Paolucci, S., "On Slow Manifolds of Chemically Reactive Systems," *Journal of Chemical Physics*, Vol. 117, pp. 1492-1496, (2002).
4. Margolis, S. B., "Time Dependent Solution of a Premixed Laminar Flame," *Journal of Computational Physics*, Vol. 27, pp. 410-427, (1978).